Nitrogen-Vacancy Singlet-Manifold Ionization Energy

S.A. Wolf,[1,2,*] I. Meirzada,[1] G. Haim,[3,4] and N. Bar-Gill[1,2,3]

[1] *The Racah Institute of Physics, The Hebrew University of Jerusalem, Jerusalem 91904, Israel*

[2] *The Center for Nanoscience and Nanotechnology, The Hebrew University of Jerusalem, Jerusalem 91904, Israel*

[3] *Department of Applied Physics, Rachel and Selim School of Engineering, Hebrew University, Jerusalem 91904, Israel*

[4] *School of Physics, The University of Melbourne, Melbourne 3010, Australia*

The singlet states of the negatively charged nitrogen-vacancy centers in diamond play a key role in its optical spin control and readout. In this work, the hitherto unknown ionization energy of the singlet is measured experimentally and found to be in the range 1.91–2.25 eV. This is obtained by analyzing photoluminescence measurements incorporating spin control and nitrogen-vacancy charge state differentiation, along with simulations based on the nitrogen-vacancy's master equation. This work establishes a protocol for a more accurate estimate of this ionization energy, which can possibly lead to improved readout methods.

I. INTRODUCTION

Negatively charged nitrogen-vacancy (N-V^-) centers are point defects in diamond which show promising quantum properties essential for various applications, ranging from magnetic sensing to quantum computing. These applications rely on the N-V center's exceptionally long coherence times and optical spin readout, even at room temperature. The properties of the N-V center are constantly being studied to improve its coherence time and readout signal-to-noise ratio (SNR). While most of the energy levels and transition rates have been measured, some are still unknown and may have a significant impact on our understanding of the system's dynamics.

The N-V center is a defect in diamond where two adjacent carbons are replaced by one nitrogen and a vacancy. The N-V^- has an additional electron which leads to two holes in the valence shell and an effective two-electron system. The ground state of the N-V^- is a spin-one triplet with a 2.87-GHz zero-field-splitting between spin projections $m_s = 0$ and $m_s = \pm 1$, and can be controlled using a resonant microwave (MW) drive. These spin states are located 2.6 eV below the conduction band (Fig. 1). The electronically excited triplet state is located 1.945 eV above the ground state with a lifetime of approximately 13 ns [1,2]. The radiative transition between the two triplet states is dominated by the phonon side band (PSB), with emission between about 650–800 nm. The N-V^- has an additional singlet (spin-zero) manifold consisting of two

energy levels that are separated by 1.19 eV with an excited state lifetime of approximately 0.1 ns [3–6]. Spin-selective intersystem crossing (ISC) allows the excited triplet to decay nonradiatively to the singlet excited state predominantly from the $m_s = \pm 1$ spin projection. The ground singlet state, commonly referred to as a metastable state due to its long lifetime (around 300 ns), decays back to the ground triplet state. Theoretical studies have predicted different values for the energy of the singlet state [7–16]. However, the energy gap between the singlet manifold and the conduction band has yet to be measured experimentally, and is the focus of this work. The N-V^- can also be ionized optically, and convert to a neutral nitrogen-vacancy (N-V^0) center which has an energy gap of 2.16 eV between its ground and excited states.

The most commonly used readout method at room temperature is based on collecting photoluminescence (PL) from the PSB while exciting the triplet transition using the PSB (typically at 532 nm) [17]. Due to the spin-selective ISC, the number of photons emitted depends on the initial spin projection of the ground triplet state. However, this readout method yields a very poor SNR and requires thousands of repetitions [17]. Different readout methods have been proposed in order to increase the readout SNR [17,18], but those readout methods all rely on the spin-dependent transition to the metastable singlet state. Better knowledge of the energy levels and transition rates, and specifically the unknown singlet energy, will allow more accurate modeling of the N-V dynamics and may lead to the development of improved readout methods. Theoretical studies have predicted various values for
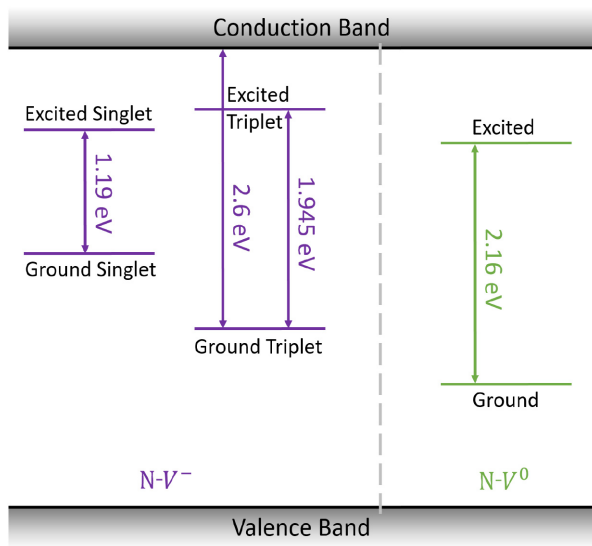
———————
*sigal.wolf@mail.huji.ac.il

FIG. 1.   Known energy levels of N-V centers.

the energy of the singlet state, and experimental data are required in order to constrain this parameter [7–14,16]. In a recent paper [19] an experimental protocol for finding the ionization energy of the singlet level was proposed by the authors. The main idea behind this protocol is to maximally populate the singlet level before applying an ionization laser pulse at varying wavelengths to check for ionization (from N-V^- to N-V^0). An analysis of the nitrogen-vacancy's master equation predicts significantly different results between ionization pulse wavelengths below and above the ionization energy. In this work we report experimental results toward a direct measurement of the singlet ionization energy and provide experimental bounds to the singlet energy. Our measurement and analysis include important modifications on the original experiment proposal.

The paper is organized as follows. We first detail the experimental protocol and pulse sequence used. We then describe the measured results, mostly of the ionization ratio normalized to different spin initializations, as a function of ionization laser power. We present the detailed measurement results, along with comparisons to simulations, in separate sections based on the ionization laser wavelength. Finally, we summarize and conclude.

II. PULSE SEQUENCE

The pulse sequence in the following measurements begins with an initialization to the ground state's $m_s = \pm 1$ spin projection, that is, initialization to spin projection $m_s = 0$ with a long 532-nm pulse followed by a π pulse using resonant MW. Next, a short 532-nm population pulse optimized to maximally populate the ground singlet state is applied (200 µW for 400 ns; see Appendix B for details), followed by a delay of approximately 30 ns to allow the triplet excited states to fully decay to either the singlet or ground triplet states. At this point the singlet is maximally populated and an ionization pulse is applied while the singlet is still highly populated (approximately 100 ns). Finally, a 532-nm readout pulse is applied, during which the emitted N-V^- PL is collected using a 650-nm long-pass filter (see Fig. 2 in Ref. [19]).

Assuming the singlet manifold lies between the ground and excited triplet states, the ionization energy of the ground singlet state is bound between 1.84 eV, corresponding to 674 nm, and 2.6 eV, corresponding to 477 nm [19]. In the following experiments we use a pulsed supercontinuum laser (NKT Photonics, WL-SC-400-15-PP) followed by different bandpass filters (blue, 500 ± 20 nm; green,
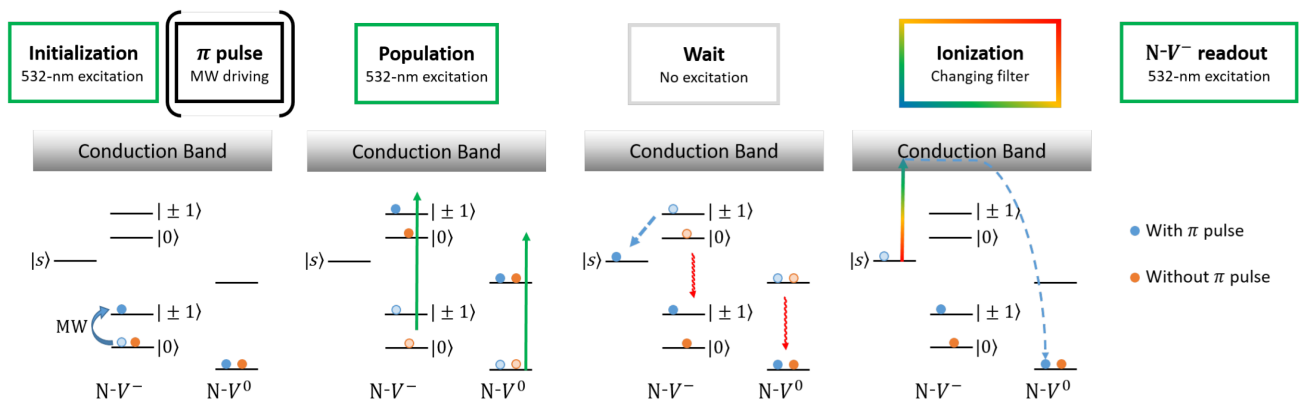

FIG. 2.   The N-V center's dynamics during the pulse sequence. Blue (orange) dots represent the population with (without) a π pulse in the initialization step. The faded dots are a reminder of the population before the current pulse. The main difference between the dynamics with and without a π pulse lies in the wait time between the population and ionization pulses, where the singlet is populated only in the case of a π pulse in the initialization. For simplicity, the ionization pulse shows only the potential ionization from the singlet. Depending on the wavelength, additional transitions may occur during this pulse such as N-V^-/N-V^0 excitation and ionization/recombination from the excited states (which are not shown in this figure).

550 ± 20 nm; red, 650 ± 20 nm; long red, 676 ± 4 nm) and a near-infrared (NIR) 976 nm continuous-wave laser (BL976-PAG900) for the ionization pulse. The long red filter and NIR laser are not expected to ionize from the singlet ground state and were added as control measurements. The experiments were conducted on a diamond sample with a high density of N-V centers. During the experiment the PL was measured as a function of the ionization pulse power. A reference measurement without a π pulse in the first initialization step (i.e., initialized to $m_s = 0$ in the first step of the experiment) was conducted for every ionization laser power in order to help isolate the singlet contribution from the rest of the N-V dynamics. The results both with and without the π pulse are normalized by the PL measurement without an ionization pulse (ionization pulse power = 0 mW), and with the same initial state. In the following section we present the PL as a function of the ionization pulse power with different filters, as well as the ratio between the experimental results with and without the π pulse in the initialization step (which will be referred to as the PNP ratio). The pulse sequence described here is the same as suggested in [19] with the addition of the reference measurement without the π pulse. Additional calibration experiments were done to maximize the singlet population during the ionization pulse, when there is a π pulse in the initialization.

III. RESULTS

Figure 3 presents the PNP ratio as a function of the ionization pulse power, allowing us to visually compare the different wavelength results. This summarizes the measurements (detailed below) and provides one of the main
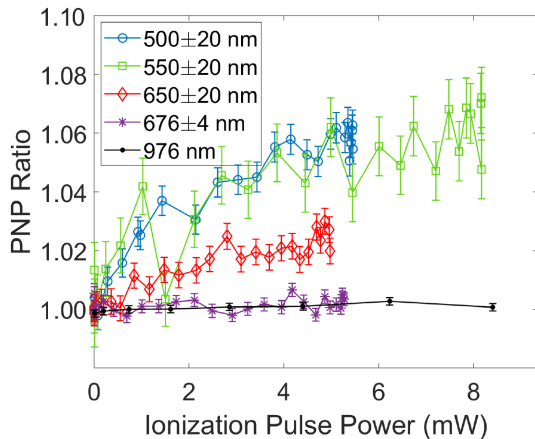

FIG. 3. PNP ratio experimental results. The ratio between experimental results with and without a π pulse in the initialization step with different ionization laser filters. Blue circles show experimental results with blue filter, green squares with green filter, red diamonds with red filter, purple stars with long red filter, and black dots with NIR laser. The solid lines were added between the experimental measurements as a visual aid.

results of this work. The results with green and blue ionization pulses show very similar behavior, suggesting they have the same (or very similar) singlet ionization cross sections (SICSs). The PNP ratio with the red filter increases less than with the blue and green filters. However, since the red filter no longer excites the N-V^0 ground state, a more careful analysis is needed to interpret this effect. The PNP results of the two control experiments, presented as purple (long red) and black (NIR) curves, show little to no increase and are approximately 1 for all laser powers, as expected (since they do no excite both N-V charge states).

In this section we compare the experimental results with simulations, and fit the SICSs in order to obtain a clear conclusion regarding the ionization energy. The simulations are based on the N-V center's master equation (detailed in Appendix A). Since we use a 532-nm excitation in all the experiments we start by examining the green filter.

A. Green (550 ± 20 nm)

Figures 3 (green line) and 4(a) show the experimental results and simulations of the PNP ratio with a green ionization pulse, respectively. For these simulations we assume that the green filter and 532-nm excitation laser have the same SICS. We can see that if there is no ionization from the singlet (SICS = 0) with this filter the PNP ratio should decrease as a function of the ionization pulse power and be less than 1. The increase in the PNP ratio in the experimental results indicates that there is a nonzero ionization cross section from the singlet. We can therefore conclude that the singlet ionization energy must be less than about 2.25 eV (corresponding to 550 nm).

We note that the PNP ratio in the simulation seems to reach a saturation value faster than in the experimental results. This could be the result of the focal spot of the ionization laser not being diffraction limited and the use of a very dense N-V sample; both would lead to an effectively lower excitation power. Therefore, an ionization power scaling parameter was added to our simulations.

In order to obtain the value of the green SICS we consider the experimental results with and without the π pulse separately, depicted in Fig. 4(b). Based on these data, we find the best-fitting parameters for the green filter to be SICS = 20.0 ± 0.5 MHz/mW and power scaling = 0.11 ± 0.0015. These simulation results are also shown in Fig. 4(b), as solid blue (π pulse) and dashed red (no π pulse) lines. In the following sections we will assume that SICS = 20 MHz/mW for the 532-nm excitation laser. We note that the simulation assumes a perfect π pulse and therefore the real SICS might be slightly higher than our extracted value.

B. Blue (500 ± 20 nm)

As discussed above, the experimental PNP ratios with blue and green ionization filters (blue and green lines in
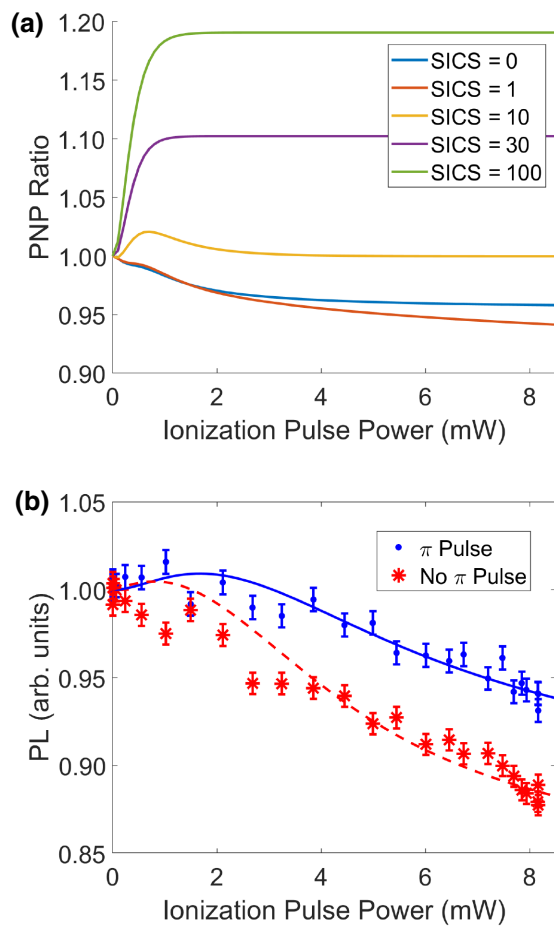
FIG. 4. Simulation and experimental results with green filter. Simulations assume the green filter and the 532-nm excitation laser have the same SICS. (a) Simulation of PNP ratio with different SICSs. Values of SICSs in legend are in units of MHz/mW. (b) Experimental results with (blue dots) and without (red stars) π pulse and simulations using fitted parameters for power factor and SICS (blue solid line, with π pulse; red dashed line, without π pulse).
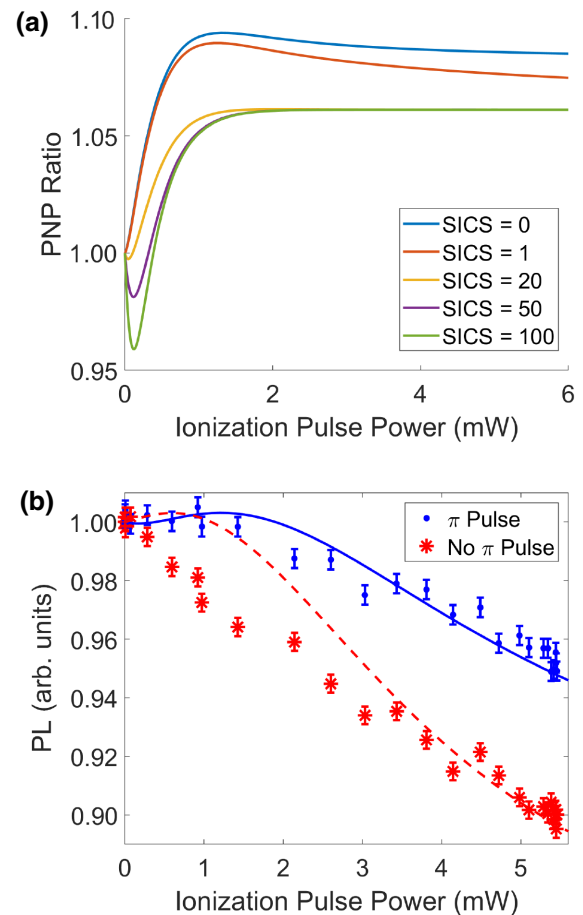
FIG. 5. Simulation and experimental results with blue filter. Simulations assume a SICS of 20 MHz/mW for the 532-nm excitation laser. (a) Simulation of PNP ratio with different SICSs. Values of SICSs in legend are in units of MHz/mW. (b) Experimental results with (blue dots) and without (red stars) π pulse and simulations using fitted parameters for power factor and blue SICS (blue solid line, with π pulse; red dashed line, without π pulse).

Fig. 3, respectively) almost all fall within the error bars of one another. Assuming the N-V excitation rates and ionization/recombination rates from the excited states with the blue filter are the same as the green, this indicates that the blue SICS and green SICS are about the same. This can also be seen from Fig. 5(a), in which we show simulations of the PNP ratio with a blue ionization pulse and different blue SICSs. For small SICS values the simulations show a maximum that does not appear in the data, while for large enough SICS values the PNP ratio decreases below 1, which is also inconsistent with the data.

Assuming that the N-V excitation and ionization/recombination rates with the blue filter are the same as the green, we fit the simulations with and without π pulse to the data separately [Fig. 5(b)]. As with the green ionization pulse, we have two fitting parameters, the blue SICS and

power scaling. The fit gives an optimum at blue SICS of 22.8 ± 0.8 MHz/mW and power scaling of 0.129 ± 0.004. As expected, the blue and green SICSs are equal within error bars. We note that the scaling factor is affected by wavelength, wavelength distribution and beam shape when using the different filters. Therefore it is not expected to have the exact same value when changing filters.

C. Red (650 ± 20 nm)

The experimental results with the red filter are shown in Figs. 3 (red line) and 6. As with the shorter wavelengths, the ratio here is also greater than 1 and increases with the ionization pulse power, but this increase is less significant. Note that this filter can excite the N-V^- triplet ground state to the triplet excited state (ZPL$^-$ = 637 nm), while it *does not* excite the N-V^0 (ZPL^0 = 575 nm). The effective
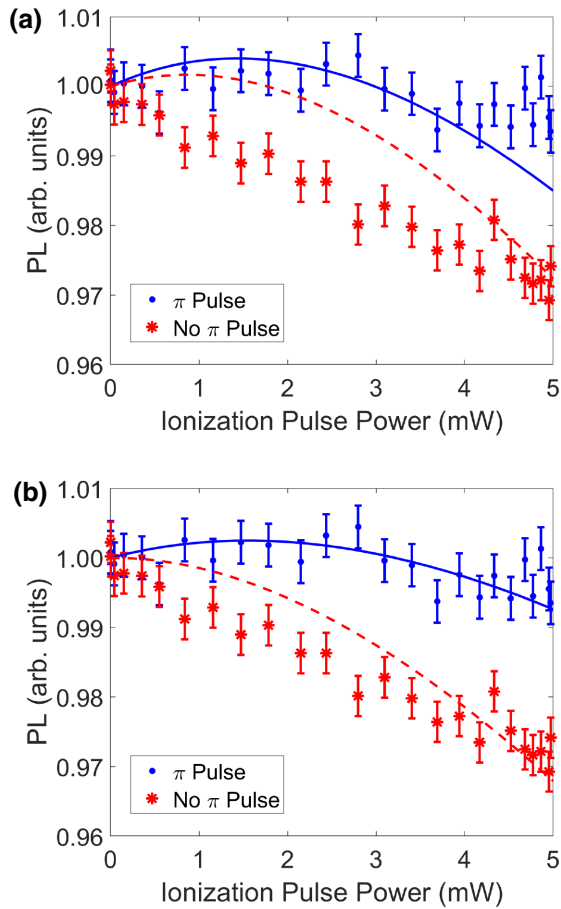
FIG. 6. Simulations and experimental results with red filter. Experimental results with and without π pulse in the initialization step (blue dots and red stars, respectively) and simulation results using fitted parameters for red SICS, red TECS, red triplet ionization cross section and red recombination from N-V^0 (with π, blue solid line; without π, red dashed line). Using population pulse parameters optimized (a) experimentally and (b) for the simulations.

triplet excitation cross section (TECS) with this filter was not measured directly, and is therefore another unknown parameter in our simulations (bound by the known 532-nm TECS).

Unlike with previous (bluer) wavelengths, the red SICS cannot be uniquely determined based on the PNP ratio results alone (further discussed in Appendix C). In order to determine the red SICS, we fit our simulation to the experimental results using four fitting parameters: red SICS and TECS, and red ionization and recombination rates from the excited states (N-V^- excited triplet and N-V^0 excited state, respectively). Figure 6(a) shows the fitted curve and experimental data. We assume the ionization power scaling with this filter is the same as with the green filter. We find that the optimal red SICS is $0.006^{+0.044}_{-0.006}$ MHz/mW, *meaning there is no (or negligible) ionization from the ground singlet state with this filter.* The optimal red TECS is 26 ± 5

MHz/mW, the ionization rate from the excited triplet is $8.2^{+1.0}_{-0.6}$ MHz/mW and the recombination rate from the N-V^0 excited state is $0.008^{+3.744}_{-0.008}$ MHz/mW. The red TECS is indeed smaller than the green TECS and consistent with [20]. The red ionization and recombination rates from this fit are within error between those of 532 nm and 1064 nm [21,22].

We note that there is some discrepancy between the fitted curves and experimental data. The population pulse power and duration used in the above simulations are the same as those used in the experiments. These parameters were experimentally optimized (as detailed in Appendix B) to maximize the singlet population during the ionization pulse (for the experiments with a π pulse in the initialization step). However, if we simulate the process of calibrating the population pulse parameters, we obtain somewhat different values compared to those obtained experimentally. The optimized population pulse parameters in the experiment are 400-ns pulse duration and 200-μW laser power, while with the simulation we get an optimum at 120-ns pulse duration and 220-μW laser power.

Using the optimal pulse parameters obtained with the simulation, and refitting the previous parameters to the red filter data, we get a significantly better description of the experimental data, as can be seen in Fig. 6(b). The optimal red SICS in this case is $0.0016^{+0.1296}_{-0.0016}$ MHz/mW, meaning, as before, that there is no (or negligible) ionization from the ground singlet state with this filter. The optimal red TECS is 6.2 ± 0.9 MHz/mW, the ionization rate from the excited triplet is 25^{+3}_{-2} MHz/mW and the recombination rate from the N-V^0 excited state is $0.005^{+3.619}_{-0.005}$ MHz/mW. The red TECS as well as the ionization/recombination cross sections from this fitting agree with the boundaries mentioned above. The results from this section indicate that the ionization energy is greater than about 1.91 eV (corresponding to 650 nm). Repeating the fitting with these population pulse parameters (optimized for the simulations) on experimental data obtained from other filters does not change the above conclusions, and specifically the existence of ionization for the green and blue filters.

D. Control experiments

Two control experiments where performed with a long red filter (672–800 nm bandpass filter), and an NIR 976 nm continuous-wave laser, such that for both cases the SICS should be zero. Figure 3 (purple and black lines) shows the PNP ratio with the long red filter and NIR laser, respectively. Both these ratios are about 1, with very small dependence on laser power. Since both these wavelengths do not excite the N-V center (either charge state), these results indicate that the SICS is approximately 0, as expected.
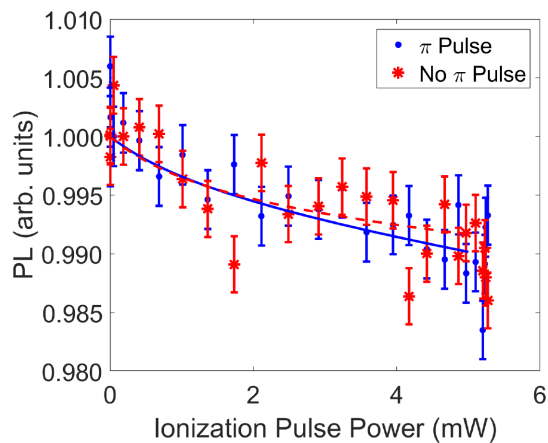
FIG. 7. Experimental results and simulations with long red filter. Experimental results with and without π pulse in the initialization step (blue dots and red stars, respectively) and simulation results using fitted parameters for long red SICS, triplet ionization cross section and recombination from N-V^0 (with π, blue solid line; without π, red dashed line).

The experimental results for the long red filter with and without a π pulse are shown in Fig. 7, with fitted simulations. If there were no population in the excited states during the ionization pulse, we would have expected to see no effect from the ionization pulse, that is, PL equals 1 independent of ionization pulse power. The small decay observed in the experiments is a result of the little population remaining in the excited states before the ionization pulse is applied. The optimal parameters found to fit these data are long red SICS equal to 0.08 ± 0.04 MHz/mW, excited triplet ionization cross section equal to 28 ± 10 MHz/mW and recombination equal to 0^{+2}_{-0} MHz/mW. For this filter the ionization power scaling was assumed to be
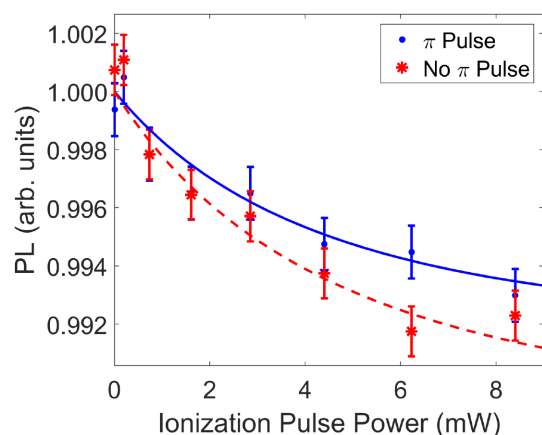

FIG. 8. NIR experimental results and simulations. Experimental results with and without π pulse in the initialization step (blue dots and red stars, respectively) and simulation results with fitted parameters with (blue solid) and without (red dashed) π pulse in the initialization step.

1. Changing the power scaling has little to no effect on the optimal long red SICS and mostly changes the optimal triplet ionization cross section. As expected, the optimal SICS is very close to zero.
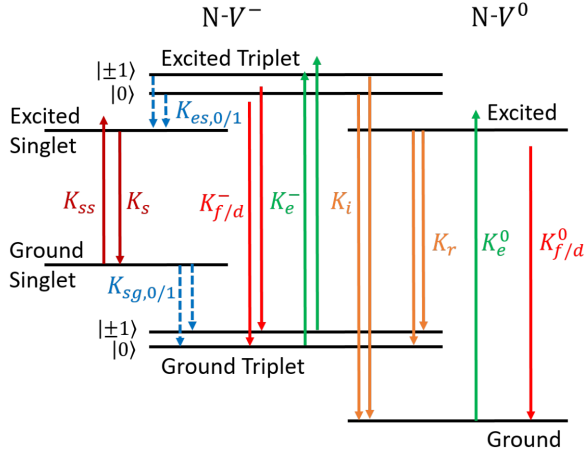
Figure 8 depicts the experimental results and simulations with fitted parameters for the NIR laser. The simulations include excitation of the singlet ground state to the singlet excited state with NIR [5], but do not include an ionization rate from the excited singlet state with NIR since this effect should be negligible given the experiment's ionization powers [23]. The fitting shows optimal NIR SICS equal to $0.002^{+0.05}_{-0.002}$ MHz/mW, NIR ionization from N-V^- excited triplet equal to 13^{+10}_{-4} MHz/mW, and NIR recombination from N-V^0 excited state equal to $0.2^{+1.3}_{-0.2}$ MHz/mW. The optimal NIR SICS is consistent with zero, as expected.

IV. SUMMARY

In this work we develop a tailored protocol to spectroscopically identify the N-V^- singlet energy levels, and implement it by measuring the N-V photodynamics as a function of various ionization wavelengths. Our results impose bounds on these energy levels, placing the ground singlet level between 1.91 and 2.25 eV below the conduction band.

We have followed the protocol suggested in [19] and incorporated several required modifications. Our results are in agreement with the theoretical predictions of [12,13, 15], and significantly improve our ability to pinpoint the singlet energy level. Additional experiments in the remaining energy range and with narrower filters (or a tunable laser) could impose an even tighter bound on the ionization energy range of the singlet.

An accurate measurement of the singlet energy level and ionization cross section as advanced in this work could lead to important applications, such as enhancing existing readout methods. Spin-to-charge conversion (SCC) readout strongly relies on the ability to induce ionization from the triplet states without affecting the singlet population [24–27]. This method commonly uses a 592-nm laser for the charge readout and in some cases for the triplet ionization pulse as well [26,27] . However, this wavelength may still induce ionization from the singlet. Narrowing the singlet ionization energy boundaries may allow optimization of the wavelength used during the SCC ionization pulse. Furthermore, recent results using photoelectric detection have shown cases with increased photoelectric current from spin projection $m_s = \pm 1$ compared to $m_s = 0$ [28]. This may be a result of singlet ionization as well as the known dependence of the triplet ionization and recombination rates on the depth of the N-V [21]. Finding the SICS in shallow N-Vs may allow better modeling and understanding of these experimental results.

FIG. 9. N-V center energy levels diagram and transitions.

TABLE II. The internal N-V^- and N-V^0 excitation rates, and ionization and recombination rates used in the simulations for the different wavelengths [21,30]. The rates in this table are in units of MHz/mW, and were multiplied by the excitation power in the master equation.

Transition	Green/blue	Red	Long red	NIR
K_e^-	135	fitted	0	0
K_e^0	243	0	0	0
K_{ss}	0	0	0	0.92
K_i	43	43 (fitted)	fitted	fitted
K_r	17.75	17.75 (fitted)	fitted	fitted
K_d^-	0	10	30	0
K_d^0	0	18	12	0

The N-V dynamics is governed by the following master equation:

$$\dot{P}_{g,0}^- = -K_e^- P_{g,0}^- + (K_f^- + K_d^-)P_{e,0}^- + K_{sg,0}P_{g,s}^- + K_r P_e^0,$$

$$\dot{P}_{g,1}^- = -K_e^- P_{g,1}^- + (K_f^- + K_d^-)P_{e,1}^- + K_{sg,1}P_{g,s}^- + K_r P_e^0,$$

$$\dot{P}_{e,0}^- = -(K_f^- + K_d^- + K_{es,0} + K_i)P_{e,0}^- + K_e^- P_{g,0}^-,$$

$$\dot{P}_{e,1}^- = -(K_f^- + K_d^- + K_{es,0} + K_i)P_{e,1}^- + K_e^- P_{g,1}^-,$$

$$\dot{P}_{e,s}^- = -K_s P_{e,s}^- + K_{ss}P_{g,s}^- + K_{es,0}(P_{e,0}^- + P_{e,1}^-),$$

$$\dot{P}_{g,s}^- = -(K_{sg,0} + K_{sg,1} - K_{ss})P_{g,s}^- + K_s P_{e,s}^-,$$

$$\dot{P}_g^0 = -K_e^0 P_g^0 + (K_f^0 + K_d^0)P_e^0 + K_i(P_{e,0}^- + P_{e,1}^-),$$

$$\dot{P}_e^0 = -(K_f^0 + K_d^0 + 2K_r)P_e^0 + K_e^0 P_g^0.$$

The populations of the N-V states are denoted by $P_n^{0/-}$, where the upper index indicates the charge state of the N-V. The letter g (e) in the lower index stand for the ground (excited) state, singlet states are denoted by s in

APPENDIX A: MASTER EQUATION AND RATES

The N-V center eight-level model as was simulated in this paper is described in Fig. 9.

TABLE I. The internal N-V^- and N-V^0 decay rates that were used to simulate the N-V center's dynamics [6,21,31,32].

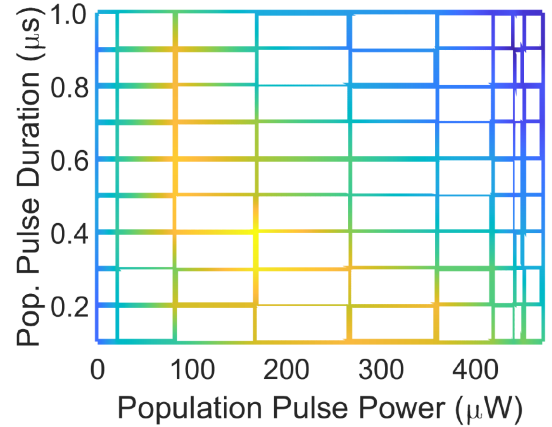| Transition	Rate (MHz)
K_f^-	77
K_f^0	53
$K_{es,0}$	0
$K_{es,1}$	30
K_s	10 000
$K_{sg,0}$	3.3
$K_{sg,1}$	0

FIG. 10. Optimization of population pulse parameters. PL from the singlet transition (proportional to singlet population during ionization pulse) as a function of pulse duration and power.

the lower index, and triplet spin projection is denoted by 0 (1) for $m_s = 0$ ($m_s = \pm1$). The rates are denoted by the letter K and are specified in Fig. 9. The simulations rely on previously published charge dynamics [21], recently measured singlet decay rate [6], and internal N-V^- rates from [29], and stimulated emission cross sections from [30], as detailed in Tables I and II.

APPENDIX B: POPULATION PULSE CALIBRATION

We tried to maximize the population of the singlet during the ionization pulse in order to get a maximal contrast. The singlet population was measured by excitation of the singlet transition (976 nm, off- resonance excitation) and collection of the singlet's PSB (1000-nm long pass filter), which will be referred to as singlet readout.

The power and duration of the population pulse were optimized together as they depend on each other. The

optimization was done using the same pulse sequence as the singlet ionization experiment described in the main text, except that the readout was done during the ionization pulse and measured the singlet population (singlet readout). The population pulse duration and power were changed throughout the experiment to measure their effect on the singlet population during the ionization pulse. As can be seen in Fig. 10, the optimal population pulse duration is 400 ns, with 200-μW excitation laser power.

APPENDIX C: RED FILTER PNP SIMULATION

Figure 11 presents the PNP simulation results with a red ionization pulse and shows a strong dependence of the results on the red SICS and TECS, respectively. These simulations assume that the ionization and recombination rates from the excited states are the same as those with a 532-nm laser [21]. Assuming the red TECS equals 1 MHz/mW [Figure 11(a)], one may conclude that the red SICS must be less than 0.5 MHz/mW, to obtain the experimentally observed increase in the PNP ratio as a function of ionization pulse power. However, one could assign the red SICS a value of 5 MHz/mW [Figure 11(b)], and by changing the red TECS, a PNP ratio greater than 1 can be achieved. Thus the red SICS cannot be uniquely determined based on the PNP ratio results alone, unlike for previous (bluer) wavelengths.
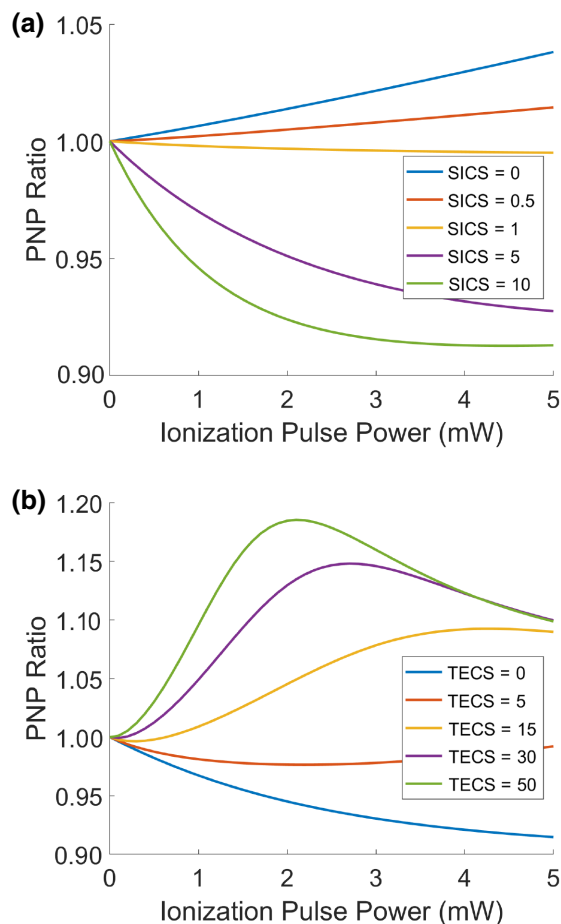

FIG. 11. Simulations with red filter. (a) PNP ratio simulations assuming TECS equal to 1 MHz/mW and different values for red SICS. Values of SICS in legend are in units of MHz/mW. (b) PNP ratio simulations assuming red SICS equal to 5 and different values of TECS. Values of TECS in legend are in units of MHz/mW.

[1] G. Davies and M. F. Hamer, Optical studies of the 1.945 eV vibronic band in diamond, Proc. R. Soc. London A **348**, 285 (1976).

[2] A. T. Collins, M. F. Thomaz, and M. I. B. Jorge, Luminescence decay time of the 1.945 eV centre in type ib diamond, J. Phys. C: Solid State Phys. **16**, 2177 (1983).

[3] L. J. Rogers, S. Armstrong, M. J. Sellars, and N. B. Manson, Infrared emission of the NV centre in diamond: Zeeman and uniaxial stress studies, New J. Phys. **10**, 103024 (2008).

[4] V. M. Acosta, A. Jarmola, E. Bauch, and D. Budker, Optical properties of the nitrogen-vacancy singlet levels in diamond, Phys. Rev. B **82**, 201202 (2010).

[5] P. Kehayias, M. W. Doherty, D. English, R. Fischer, A. Jarmola, K. Jensen, N. Leefer, P. Hemmer, N. B. Manson, D. Budker, *et al.*, Infrared absorption band and vibronic structure of the nitrogen-vacancy center in diamond, Phys. Rev. B **88**, 165202 (2013).

[6] R. Ulbricht and Z.-H. Loh, Excited-state lifetime of the NV$^-$ infrared transition in diamond, Phys. Rev. B **98**, 094309 (2018).

[7] A. Dräbenstedt, L. Fleury, C. Tietz, F. Jelezko, S. Kilin, A. Nizovtzev, and J. Wrachtrup, Low-temperature microscopy and spectroscopy on single defect centers in diamond, Phys. Rev. B **60**, 11503 (1999).

[8] A. Gali, M. Fyta, and E. Kaxiras, Ab initio supercell calculations on nitrogen-vacancy center in diamond: Electronic structure and hyperfine tensors, Phys. Rev. B **77**, 155206 (2008).

[9] A. S. Zyubin, A. M. Mebel, M. Hayashi, H. C. Chang, and S. H. Lin, Quantum chemical modeling of photoadsorption properties of the nitrogen-vacancy point defect in diamond, J. Comput. Chem. **30,** 119 (2009).

[10] P. Delaney, J. C. Greer, and J. A. Larsson, Spin-polarization mechanisms of the nitrogen-vacancy center in diamond, Nano Lett. **10,** 610 (2010).

[11] D. M. Toyli, D. J. Christle, A. Alkauskas, B. B. Buckley, C. G. Van de Walle, and D. D. Awschalom, Measurement and Control of Single Nitrogen-Vacancy Center Spins above 600 K, Phys. Rev. X **2,** 031001 (2012).

[12] M. L. Goldman, M. W. Doherty, A. Sipahigil, N. Y. Yao, S. D. Bennett, N. B. Manson, A. Kubanek, and M. D. Lukin, State-selective intersystem crossing in nitrogen-vacancy centers, Phys. Rev. B **91,** 165201 (2015).

[13] M. L. Goldman, A. Sipahigil, M. W. Doherty, N. Y. Yao, S. D. Bennett, M. Markham, D. J. Twitchen, N. B. Manson, A. Kubanek, and M. D. Lukin, *et al.*, Phonon-Induced Population Dynamics and Intersystem Crossing in Nitrogen-Vacancy Centers, Phys. Rev. Lett. **114,** 145502 (2015).

[14] L. J. Rogers, M. W. Doherty, M. S. J. Barson, S. Onoda, T. Ohshima, and N. B. Manson, Singlet levels of the NV^- centre in diamond, New J. Phys. **17,** 013048 (2015).

[15] G. m. H. Thiering and A. Gali, Theory of the optical spin-polarization loop of the nitrogen-vacancy center in diamond, Phys. Rev. B **98,** 085207 (2018).

[16] C. Bhandari, A. L. Wysocki, S. E. Economou, P. Dev, and K. Park, Multiconfigurational study of the negatively charged nitrogen-vacancy center in diamond, Phys. Rev. B **103,** 014115 (2021).

[17] D. Hopper, H. Shulevitz, and L. Bassett, Spin readout techniques of the nitrogen-vacancy center in diamond, Micromachines **9,** 437 (2018).

[18] I. Meirzada, S. A. Wolf, A. Naiman, U. Levy, and N. Bar-Gill, Enhanced spin state readout of nitrogen-vacancy centers in diamond using infrared fluorescence, Phys. Rev. B **100,** 125436 (2019).

[19] I. Meirzada, S. A. Wolf, and N. Bar-Gill, Finding the nitrogen-vacancy singlet manifold energy level using charge-conversion pulse sequences, Phys. Rev. B **104,** 155413 (2021).

[20] S. D. Subedi, V. V. Fedorov, J. Peppers, D. V. Martyshkin, S. B. Mirov, L. Shao, and M. Loncar, Laser spectroscopic characterization of negatively charged nitrogen-vacancy (NV^-) centers in diamond, Opt. Mater. Express **9,** 2076 (2019).

[21] I. Meirzada, Y. Hovav, S. A. Wolf, and N. Bar-Gill, Negative charge enhancement of near-surface nitrogen vacancy centers by multicolor excitation, Phys. Rev. B **98,** 245411 (2018).

[22] K. Beha, A. Batalov, N. B. Manson, R. Bratschitsch, and A. Leitenstorfer, Optimum Photoluminescence Excitation and Recharging Cycle of Single Nitrogen-Vacancy Centers in Ultrapure Diamond, Phys. Rev. Lett. **109,** 097404 (2012).

[23] D. A. Hopper, R. R. Grote, A. L. Exarhos, and L. C. Bassett, Near-infrared-assisted charge control and spin readout of the nitrogen-vacancy center in diamond, Phys. Rev. B **94,** 241201 (2016).

[24] B. J. Shields, Q. P. Unterreithmeier, N. P. de Leon, H. Park, and M. D. Lukin, Efficient Readout of a Single Spin State in Diamond via Spin-to-Charge Conversion, Phys. Rev. Lett. **114,** 136402 (2015).

[25] J.-C. Jaskula, B. Shields, E. Bauch, M. Lukin, A. Trifonov, and R. Walsworth, Improved Quantum Sensing with a Single Solid-State Spin via Spin-to-Charge Conversion, Phys. Rev. Appl. **11,** 064003 (2019).

[26] H. Jayakumar, S. Dhomkar, J. Henshaw, and C. A. Meriles, Spin readout via spin-to-charge conversion in bulk diamond nitrogen-vacancy ensembles, Appl. Phys. Lett. **113,** 122404 (2018).

[27] R. Giri, R. H. Jensen, D. Khurana, J. Bocquel, I. P. Radko, J. Lang, C. Osterkamp, F. Jelezko, K. Berg-Sorensen, U. L. Andersen, and A. Huck, Charge stability and charge-state-based spin readout of shallow nitrogen-vacancy centers in diamond (2022).

[28] E. Bourgeois, J. Soucek, J. Hruby, M. Gulka, and M. Nesladek, Photoelectric detection of nitrogen-vacancy centers magnetic resonances in diamond: Role of charge exchanges with other optoelectrically active defects, Adv. Quantum Technol. **5,** 2100153 (2022).

[29] L. Robledo, H. Bernien, T. van der Sar, and R. Hanson, Spin dynamics in the optical cycle of single nitrogen-vacancy centres in diamond, New J. Phys. **13,** 025013 (2011).

[30] E. Fraczek, V. G. Savitski, M. Dale, B. G. Breeze, P. Diggle, M. Markham, A. Bennett, H. Dhillon, M. E. Newton, A. J. Kemp, *et al.*, Laser spectroscopy of NV- and NV0 colour centres in synthetic diamond, Opt. Mater. Express **7,** 2571 (2017).

[31] N. B. Manson, J. P. Harrison, and M. J. Sellars, Nitrogen-vacancy center in diamond: Model of the electronic structure and associated dynamics, Phys. Rev. B **74,** 104303 (2006).

[32] G. Liaugaudas, G. Davies, K. Suhling, R. U. A. Khan, and D. J. F. Evans, Luminescence lifetimes of neutral nitrogen-vacancy centres in synthetic diamond containing nitrogen, J. Phys.: Condens. Matter **24,** 435503 (2012).